BULLETIN OF THE POLISH ACADEMY OF SCIENCES
TECHNICAL SCIENCES,
DOI:10.24425/bpasts.2026.158307

Prediction of adsorption efficiency for alkali activated carbon using Artificial Neural Networks

Abdelrahman G. Gadallah*[1], AbdulAziz A. AlGhamdi[1], and H. E. Fawaz [2]

[1]Department of Chemical Engineering, College of Engineering, Imam Mohammad Ibn Saud Islamic University (IMSIU), 11432 Riyadh, Saudi Arabia.
[2]Department of Mechanical Engineering, National Research Centre, Giza 12622, Egypt

Abstract. Activated carbon is a widely used adsorbent in wastewater treatment due to its high surface area and tunable physicochemical properties. The adsorption performance of activated carbon is strongly influenced by synthesis parameters, including impregnation ratio, activation time, and activation temperature, which are studied in detail in the present work. An artificial neural network (ANN) model was developed to predict the adsorption capacity of methylene blue based on these three process variables. Activated carbons were prepared using chemical activation with potassium hydroxide (KOH) and sodium hydroxide (NaOH), and their adsorption performance was determined through experimental measurements. The ANN model adopted a multilayer perceptron (MLP) architecture with an input layer consisting of three neurons corresponding to impregnation ratio, activation time, and activation temperature. This was followed by ten hidden layers, each containing fourteen neurons, and a single output neuron representing the adsorption capacity in mg/g. The network was trained using backpropagation and optimized using the ADAM optimizer. The architecture and the number of neurons were selected through successive comparison of the loss values on training and validation datasets to ensure high generalization accuracy. The trained ANN model accurately captured the nonlinear relationships between synthesis parameters and adsorption capacity. This work highlights the capability of ANN as an effective predictive tool in materials science, facilitating the design and optimization of activated carbon synthesis with reduced experimental effort. The proposed approach can serve as a foundation for developing intelligent systems for material selection and process optimization in environmental applications.

Key words: Activated Carbons; Adsorption Capacity; Artificial neural network; Multilayer perceptron; Backpropagation algorithm; Adam optimizer

1. INTRODUCTION

The rapid expansion of industrial activities, particularly in textile, paper, pharmaceutical, and chemical manufacturing sectors, has led to the continuous discharge of dye-contaminated wastewater into aquatic environments. Synthetic dyes are highly stable, contain complex aromatic structures, and resist biodegradation, making their removal from effluents a significant environmental challenge. Among these dyes, methylene blue (MB) is commonly detected in industrial wastewater, and even at low concentrations, can reduce light penetration, disrupt photosynthesis, and pose toxic or mutagenic risks to aquatic organisms and human health [1, 2, 3, 4, 5, 6]. Therefore, the efficient removal of methylene blue from wastewater is of critical environmental and regulatory importance.

Various physical, chemical, and biological methods have been developed for dye removal, including coagulation–flocculation, membrane separation, advanced oxidation processes, electrochemical treatment, and biological degradation [7, 8, 9, 10, 11, 12]. However, these approaches often suffer from high operational costs, incomplete dye removal, secondary waste generation, membrane fouling, or sensitivity to wastewater composition. Adsorption has emerged as one of the most efficient and widely used methods due to its operational simplicity, high removal efficiency, and flexibility over a wide concentration range. Among adsorbents, activated carbon is the most widely employed owing to its high specific surface area, tunable pore structure, and strong affinity toward organic pollutants [13, 14, 15, 16, 17, 18]. The global market for activated carbon is projected to reach USD 5,497.3 million by 2033, growing at a CAGR of 4.0% from 2026 to 2033 driven by stringent environmental regulations and growing industrial demand for clean water and air [19].

The adsorption of methylene blue onto activated carbon occurs through multiple mechanisms, including electrostatic interactions, π–π stacking between aromatic rings, hydrogen bonding, and pore-filling effects [20, 21, 22, 23, 24, 25]. The relative contribution of each mechanism is strongly influenced by the surface chemistry and pore architecture of the carbon. Adsorption kinetics are further affected by mass transfer limitations such as external film diffusion, intraparticle (pore) diffusion, and surface reaction steps [26]. A deep understanding of these mechanisms is essential for optimizing adsorption performance, yet traditional experimental approaches alone often fail to fully capture the complex interplay of synthesis parameters.

The physicochemical properties of activated carbon are highly sensitive to the synthesis route and activation conditions. Chemical activation using alkali agents such as potassium hydroxide (KOH) and sodium hydroxide (NaOH) is widely reported as an effective method to produce activated carbons with high surface area and well-developed microporosity [27, 28, 29, 30, 31]. During alkali activation, hydroxide ions react with the carbon precursor, promoting dehydration, gasification, and intercalation of alkali metals, resulting in pore formation and widening. Key synthesis parameters—including impregnation ratio, activation temperature,

*e-mail: Agadallah@imamu.edu.sa

and activation time—control these reactions and ultimately determine pore size distribution, surface functional groups, and adsorption capacity [32, 33, 34, 35]. Optimizing these parameters using conventional experimental methods is challenging due to their nonlinear and interdependent effects.

To overcome these challenges, data-driven modeling approaches, particularly artificial intelligence (AI) methods, have been increasingly applied in adsorption studies. Among them, artificial neural networks (ANNs) are particularly suitable for modeling nonlinear systems due to their ability to learn complex input–output relationships directly from experimental data without requiring explicit mechanistic assumptions [36, 37, 38, 39, 40, 41]. ANNs have been successfully employed to predict adsorption capacity, removal efficiency, kinetic parameters, and equilibrium behavior for a wide variety of adsorbent–adsorbate systems [42, 43, 44, 45, 46, 47]. Compared to traditional regression or empirical models, ANNs provide superior predictive accuracy, especially when the system exhibits strong nonlinearity and parameter coupling.

Recent advances in deep learning have shown that deeper multilayer perceptron (MLP) architectures can further enhance predictive performance by capturing hierarchical interactions between synthesis parameters and adsorption behavior [48, 49, 50, **?**, 51]. Conceptually, the input layer of an ANN represents the macroscopic synthesis variables that dictate material formation, the hidden layers encode complex interactions associated with pore structure evolution, surface functionalization, and adsorption site accessibility, and the output layer predicts the macroscopic adsorption capacity, linking synthesis conditions to performance without explicit physical equations. This hierarchical learning capability provides both predictive power and an interpretable framework that aligns with multiscale adsorption phenomena.

Despite these advances, comparative ANN modeling of activated carbons prepared using different alkali activators under consistent network architectures remains underexplored. Most existing studies focus on a single activation route or employ shallow networks, limiting their ability to isolate the influence of activation chemistry on adsorption performance. Developing separate deep ANN models for KOH- and NaOH-activated carbons allows for capturing their distinct adsorption characteristics while maintaining consistent architecture, training protocols, and hyperparameters. This approach facilitates direct comparison of activation chemistry effects on adsorption behavior and supports generalizable insights for materials design.

In this study, a deep MLP-based ANN model is developed to predict the adsorption capacity of methylene blue onto activated carbons prepared via KOH and NaOH activation. Experimental adsorption data from our previous study [52] were used to train and validate the models, with impregnation ratio, activation temperature, and activation time selected as the key input variables due to their significant influence on pore development and surface chemistry.

Identical ANN architectures are employed for both activation routes to ensure methodological consistency, while separate models are trained for each activator to capture activator-specific adsorption behavior. The proposed framework demonstrates the potential of deep learning as an effective predictive and optimization tool, reducing experimental effort while providing insight into adsorption phenomena relevant to wastewater treatment applications.

2. ARTIFICIAL NEURAL NETWORK (ANN) FRAMEWORK FOR ADSORPTION CAPACITY PREDICTION

In this study, an artificial neural network (ANN) model was developed to predict the adsorption capacity of methylene blue based on three synthesis variables: impregnation ratio, activation time, and activation temperature. These variables influence the physicochemical properties of activated carbons prepared using two activating agents—potassium hydroxide (KOH) and sodium hydroxide (NaOH). Due to the nonlinear and coupled effects of these parameters, ANN serves as an efficient modeling tool to capture the underlying complex relationships. Identical ANN architectures were employed for KOH-activated and NaOH-activated carbons, including the same MLP structure, number of layers and neurons, activation functions, and training hyperparameters. However, separate models were trained using the respective experimental datasets for each activating agent, leading to distinct learned weights and biases that reflect their different adsorption behaviors.

The experimental dataset used for ANN modeling consists of 300 data points, which were randomly divided into 70% for training, 15% for validation, and 15% for testing. Although experimental datasets in activated carbon synthesis are inherently constrained by time and cost, the present dataset covers a broad and representative range of operating conditions. Specifically, the impregnation ratio varies from 1 to 6, activation time from 0.5 to 3 h, and activation temperature from 600 to 900 K, ensuring adequate diversity in the input space for both KOH- and NaOH-activated carbons. To mitigate potential overfitting associated with the use of a deep neural network, the ANN architecture was optimized through systematic evaluation of multiple network configurations using training and validation loss functions. The final model was selected based on its ability to maintain consistent performance across training, validation, and testing datasets rather than solely minimizing training error. In addition, the ANN predictions were benchmarked against a simpler quadratic regression model using multiple statistical metrics, parity plots, and error analyses. The consistently superior performance of the ANN across these independent evaluations provides strong evidence of its generalization capability and alleviates concerns related to overfitting despite the limited experimental nature of the dataset.

2.1. Network Architecture and Input Representation

The architecture of the artificial neural network (ANN) used in this study is illustrated in detail in Fig. 1 and comprises three primary components: an input layer, multiple hidden layers, and an output layer. The input layer includes three neurons, corresponding to the three experimental variables: x_1 represents the impregnation ratio, x_2 denotes the activation time (in hours), and x_3 corresponds to the activation temperature (in

degrees Celsius). All input variables were normalized using min–max scaling prior to model training to ensure that no input dominates due to numerical magnitude. Let $x \in R^3$ represent the input feature vector:

$$x = [x_1, x_2, x_3]^T \tag{1}$$

This input vector is fed into the first layer of the network and is the starting point for all computations that follow.

2.2. Hidden Layers and Neuron-Level Computations

The ANN includes 10 hidden layers, each comprising 14 neurons, making it a deep feedforward neural network. Each neuron in these hidden layers performs a two-step transformation: first, it computes a weighted sum of its inputs and adds a bias term, and second, it applies a nonlinear activation function to introduce nonlinearity into the model. The operation of a neuron in the L-th layer can be described mathematically as:

$$z_i^{(L)} = \sum_{j=1}^{n_{L-1}} w_{ij}^{(L)} a_j^{(L-1)} + b_i^{(L)} \quad for\ i = 1, 2, \ldots, 14 \tag{2}$$

$$a_i^{(L)} = f\left(z_i^{(L)}\right) \tag{3}$$

Where:
$z_i^{(L)}$ is the weighted sum for neuron i in layer L,
$w_{ij}^{(L)}$ is the weight connecting neuron j in layer $L-1$ to neuron i in layer L,
$b_i^{(L)}$ is the bias of neuron i in layer L,
$a_j^{(L-1)}$ is the output (activation) of the $j-th$ neuron from the previous layer,
f is the activation function, chosen here as ReLU (Rectified Linear Unit), defined by:

$$f(z) = \max(0, z) \tag{4}$$

The ReLU activation function is selected because of its ability to mitigate vanishing gradients and enhance convergence speed, particularly in deep networks. ReLU was employed as the activation function in the hidden layers due to its efficient gradient propagation and superior convergence performance compared to sigmoid and tanh functions for this nonlinear regression problem.

The ANN architecture was selected through systematic testing of multiple configurations with fewer hidden layers and neurons, and the final model (10 hidden layers with 14 neurons each) was chosen as it provided the lowest validation loss and best generalization performance, while simpler architectures resulted in higher prediction errors.

2.3. Output Layer and Regression Output

The final (output) layer contains a single neuron that outputs the predicted adsorption capacity $\widehat{y}$ in mg/g. Since this is a regression problem, the output layer does not apply any activation function, or equivalently, it uses a linear activation:

$$\widehat{y} = z^{(\text{out})} = \sum_{j=1}^{14} w_j^{(\text{out})} a_j^{(10)} + b^{(\text{out})} \tag{5}$$

Where:
$a_j^{(10)}$ are the activations of the 10th hidden layer,
$w_j^{(\text{out})}$ are the output weights, and
$b^{(\text{out})}$ is the output bias.
This linear output enables the ANN to produce continuous real values over a wide range, as required for modeling adsorption capacity.

2.4. Training Procedure and Loss Function

The ANN is trained using a supervised learning approach. Given a dataset of N samples, each with an input vector x_i and a corresponding target output y_i (experimentally measured adsorption capacity), the objective is to minimize the prediction error. The error is quantified by the Mean Squared Error (MSE) loss function:

$$J = \frac{1}{N} \sum_{i=1}^{N} (\widehat{y}_i - y_i)^2 \tag{6}$$

This function penalizes larger deviations between the predicted and actual values, thus guiding the network toward better accuracy.

2.5. Backpropagation and Gradient-Based Optimization

To minimize the loss function, the ANN employs the backpropagation algorithm, which calculates the gradient of the loss with respect to every weight and bias in the network using the chain rule. The error term for neuron i in layer L, denoted $\delta_i^{(L)}$, is defined as:

$$\delta_i^{(L)} = \frac{\partial J}{\partial z_i^{(L)}} = \left(\sum_k \delta_k^{(L+1)} w_{ki}^{(L+1)} \right) \cdot f'\left(z_i^{(L)}\right) \tag{7}$$

Where $f'\left(z_i^{(L)}\right)$ is the derivative of the activation function ReLU:

$$f'(z) = \begin{cases} 1 & \text{if } z > 0 \\ 0 & \text{if } z \leq 0 \end{cases} \tag{8}$$

The gradients for weights and biases are then computed as:

$$\frac{\partial J}{\partial w_{ij}^{(L)}} = \delta_i^{(L)} \cdot a_j^{(L-1)}, \quad \frac{\partial J}{\partial b_i^{(L)}} = \delta_i^{(L)} \tag{9}$$

2.6. ADAM Optimization Algorithm

The weight and bias updates are performed using the ADAM optimizer (learning rate = 0.001, batch size = 32) for a maximum of 1000 epochs, with early stopping based on validation loss to prevent overfitting. The ADAM optimizer was employed because it combines momentum and adaptive learning rate strategies, enabling stable and efficient training of deep neural networks and accelerating convergence for nonlinear regression problems based on experimental datasets. For each parameter θ, the optimizer maintains two running averages: m_t : the exponentially decaying average of past gradients (momentum),
υ_t : the exponentially decaying average of squared gradients.

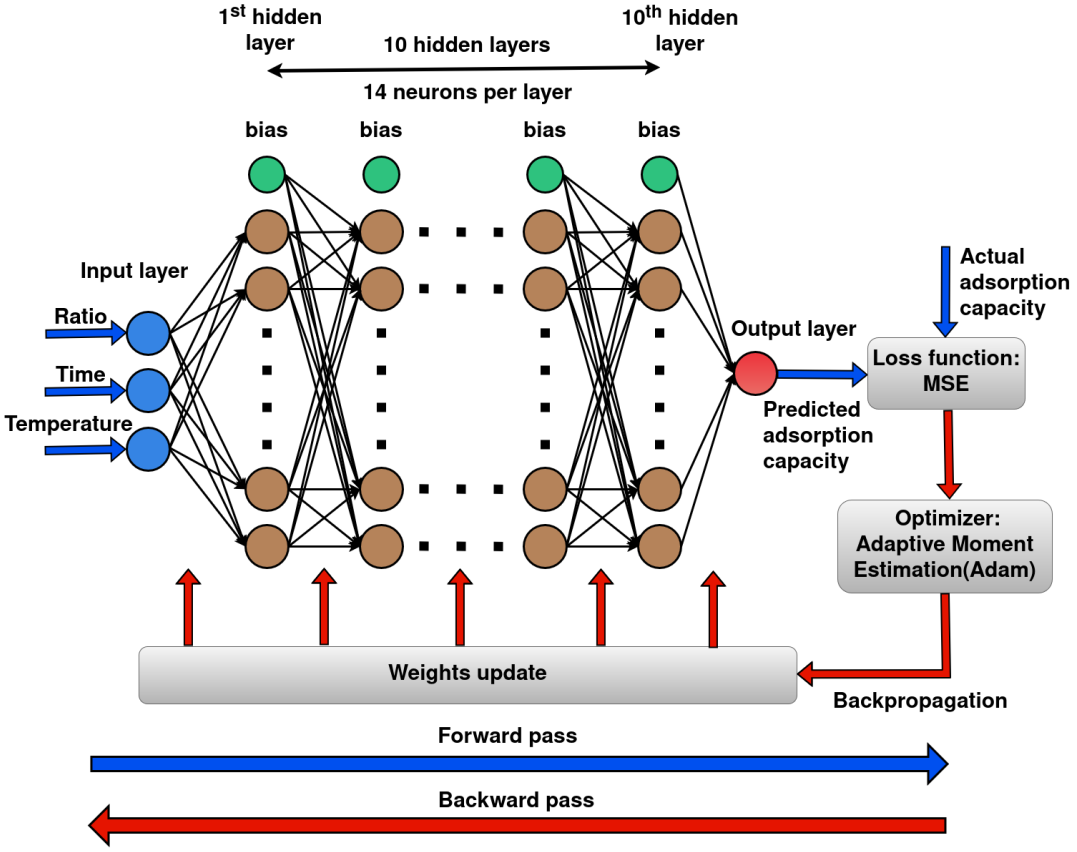

Fig. 1. Schematic diagram of the ANN architecture used in the present study

The update rules are given by:

$$m_t = \beta_1 m_{t-1} + (1-\beta_1)\nabla_\theta J_t \tag{10}$$

$$\upsilon_t = \beta_2 \upsilon_{t-1} + (1-\beta_2)(\nabla_\theta J_t)^2 \tag{11}$$

$$\widehat{m}_t = \frac{m_t}{1-\beta_1^t}, \quad \widehat{\upsilon}_t = \frac{\upsilon_t}{1-\beta_2^t} \tag{12}$$

$$\theta_{t+1} = \theta_t - \alpha \frac{\widehat{m}_t}{\sqrt{\widehat{\upsilon}_t} + \varepsilon} \tag{13}$$

where α is the learning rate, β_1 and β_2 are decay rates, and ε is a small constant for numerical stability.

2.7. Model Evaluation Metrics

To evaluate the performance of the artificial neural network (*ANN*) model developed for predicting the adsorption capacity of methylene blue, six statistical and loss-based metrics were employed: Mean Squared Error (*MSE*), Mean Absolute Percentage Error (*MAPE*), Mean Squared Logarithmic Error (*MSLE*), $Log-Cosh$ Loss, Coefficient of Determination (R^2), and Pearson Correlation Coefficient (r). These metrics collectively provided a comprehensive understanding of the model's accuracy, reliability, and generalization capability.

MSE was used as both a performance indicator and the loss function during the model's training phase. It measures the average of the squared differences between actual and predicted values, emphasizing larger errors due to the squaring operation. Its mathematical formulation is described in Eq. 6. A lower *MSE* reflects better model accuracy. Alongside this, *MAPE* was used to express the prediction error as a percentage of the actual values, enabling easier interpretation across varying data magnitudes. Its formulation is

$$\text{MAPE} = \frac{1}{N}\sum_{i=1}^{N}\left|\frac{y_i - \widehat{y}_i}{y_i}\right| \times 100\% \tag{14}$$

Where y_i and $\widehat{y}_i$ represent the actual and predicted values, respectively, and N is the total number of observations. This metric offers a scale-independent metric for relative error analysis, though it can be sensitive to small actual values.

MSLE was also included to account for the multiplicative nature of certain prediction errors, especially when actual values span several orders of magnitude. This metric evaluates the squared logarithmic differences and is defined as

$$\text{MSLE} = \frac{1}{N}\sum_{i=1}^{N}(\log(y_i+1) - \log(\widehat{y}_i+1))^2 \tag{15}$$

It penalizes underestimation less harshly than overestimation and provides smoother behavior when outputs are near zero. In addition, the $Log-Cosh$ Loss was adopted as a robust alternative to *MSE*. It behaves similarly to *MSE* for small errors but grows more slowly for large discrepancies, thereby

reducing the influence of outliers. This function is defined as

$$\text{Log-Cosh Loss} = \sum_{i=1}^{N} \log\left(\cosh\left(y_i - \widehat{y}_i\right)\right) \tag{16}$$

To assess how well the model captured the variance in the experimental data, the coefficient of determination (R^2) was calculated. was calculated. This metric is given by

$$R^2 = 1 - \frac{\sum_{i=1}^{N}\left(y_i - \widehat{y}_i\right)^2}{\sum_{i=1}^{N}\left(y_i - \bar{y}\right)^2} \tag{17}$$

Where $\bar{y}$ represents the mean of the actual values. An R^2 value closer to one indicates that a larger proportion of the variability in the output is explained by the model. Lastly, the Pearson correlation coefficient (r) was computed to quantify the strength and direction of the linear relationship between predicted and actual values. It is calculated using the formula:

$$r = \frac{\sum_{i=1}^{N}\left(y_i - \bar{y}\right)\left(\widehat{y}_i - \bar{\widehat{y}}\right)}{\sqrt{\left(\sum_{i=1}^{N}\left(y_i - \bar{y}\right)^2\right)\left(\sum_{i=1}^{N}\left(\widehat{y}_i - \bar{\widehat{y}}\right)^2\right)}} \tag{18}$$

where $\bar{y}$ and $\bar{\widehat{y}}$ are the means of the actual and predicted values, respectively. Values of r close to $+1$ indicate a strong positive correlation between predictions and experimental data.

The integration of these diverse metrics enabled a multidimensional evaluation of the *ANN* model. While *MSE*, *MSLE*, and $Log-Cosh$ Loss focused on absolute and squared errors, *MAPE* provided insights into relative deviations. R^2 and r, on the other hand, offered statistical perspectives on model fit and correlation. Together, these measures ensured that the developed ANN model not only achieved high predictive accuracy but also maintained robustness and reliability across different adsorption conditions and synthesis variables.

3. RESULTS AND DISCUSSION

3.1. Convergence analysis of ANN training process

Figure 2 illustrates the convergence behavior of the Artificial Neural Network (ANN) model over the course of 5000 training epochs for two different chemical activation cases: potassium hydroxide (KOH) and sodium hydroxide (NaOH). This figure is composed of six subfigures, each corresponding to a specific performance metric used to evaluate the training process and accuracy of the ANN model: Mean Squared Error (MSE), Mean Absolute Percentage Error (MAPE), Mean Squared Logarithmic Error (MSLE), log-cosh loss, coefficient of determination (R^2), and correlation coefficient (r). Each subfigure tracks the evolution of the respective metric as training progresses, providing insight into the convergence dynamics of the model.

Figure 2a depicts the variation of Mean Squared Error (MSE) with respect to the number of training epochs. MSE is a primary loss function that quantifies the average squared difference between predicted and actual values, making it highly sensitive to large errors. As shown, both models—one trained on KOH-activated carbon data and the other on NaOH-activated carbon data—demonstrate a clear and steady decline in MSE values as the training proceeds. This indicates that the models are effectively learning the underlying patterns in the data. After 5000 epochs, the MSE for the KOH case converges to a value of 5.416×10^{-2}, slightly lower than the NaOH case, which reaches 5.516×10^{-2}. This suggests a marginally better-fitting model in the KOH case in terms of minimizing squared prediction errors.

Figure 2b shows the evolution of the Mean Absolute Percentage Error (MAPE), which expresses prediction error as a percentage and is more interpretable when dealing with diverse scales of data. The MAPE curves for both activation agents decrease significantly during the early stages of training and eventually stabilize, reflecting consistent improvements in the model's predictive accuracy. The final MAPE for the KOH dataset is 6.416×10^{-1}, while the NaOH dataset yields a slightly lower average of approximately 6×10^{-1}. Although both models show satisfactory performance, the lower MAPE for NaOH implies slightly better relative accuracy in percentage terms.

Figure 2c presents the Mean Squared Logarithmic Error (MSLE), a metric particularly useful when the target variable spans several orders of magnitude or when underestimations should be penalized less severely. The MSLE curves for both cases remain consistently low throughout the training process, and their convergence is evident as the epochs progress. At epoch 5000, the MSLE for the KOH case is 6×10^{-6}, and for the NaOH case, it is 6.33×10^{-6}. These extremely low values demonstrate that both models are highly precise, especially in terms of small-scale variations in the adsorption capacity data.

Figure 2d illustrates the convergence of the log-cosh loss, a smooth and robust loss function that behaves like MSE for small errors but becomes linear for larger discrepancies, thus being less sensitive to outliers. The ANN model shows gradual convergence for both activation cases, with the KOH model attaining a log-cosh value of 6.25×10^{-2}, and the NaOH model reaching 7.16×10^{-2}. This again indicates that the KOH-based model demonstrates marginally better error handling and generalization.

Figure 2e provides the convergence trend of the coefficient of determination (R^2), which reflects the proportion of variance in the target variable that is predictable from the input variables. The R^2 values increase rapidly in the early epochs and plateau as the model fine-tunes its predictions. After 5000 epochs, the R^2 value for the KOH case is 0.964, indicating that 96.4% of the variability in the experimental adsorption capacity data is explained by the model. In comparison, the NaOH model achieves an R^2 of 0.957, suggesting similarly high predictive performance with a slightly lower degree of explained variance.

Finally, Figure 2f shows the Pearson correlation coefficient (r), which measures the linear correlation between predicted and actual values. Both models show strong positive correlation throughout the training period, with final r values of 0.963 for the KOH case and 0.952 for the NaOH case. These results confirm that the model's outputs align very closely with the actual experimental measurements and validate the ANN's capability in capturing the relationships among the synthesis

parameters and the adsorption performance.

In conclusion, Figure 2 collectively demonstrates that the ANN models for both KOH-and NaOH-activated carbons achieve strong convergence and excellent predictive capabilities across all performance metrics after 5000 epochs. While both chemical activations lead to highly accurate models, the KOH-based ANN exhibits slightly better performance in terms of lower error values and higher R^2 and correlation coefficients. This suggests that the ANN captures the adsorption behavior of KOH-activated carbon with slightly greater precision, possibly due to a more distinct or structured relationship between the input synthesis conditions and the output adsorption capacity in this dataset.

3.2. Effect of synthesis parameters on adsorption capacity: experimental and ANN-based evaluation

Figure 3 presents a comprehensive analysis of how three key synthesis variables—impregnation ratio (Fig. 3a), activation time (Fig. 3b), and activation temperature (Fig. 3c)—affect the adsorption capacity of methylene blue. These figures provide a side-by-side comparison between experimental values and those predicted by the ANN model for activated carbons produced using potassium hydroxide (KOH) and sodium hydroxide (NaOH). Across all three sub-figures, a strong correlation and excellent agreement can be observed between the experimental results and the ANN predictions, indicating the reliability and robustness of the developed neural network in capturing the complex relationships governing the adsorption process.

In Figure 3a, the effect of the impregnation ratio—defined as the weight ratio of chemical activating agent to precursor material—is illustrated. This ratio is a fundamental variable in the chemical activation method for synthesizing activated carbon, as it directly influences pore development and surface reactivity. The figure shows that, for both KOH and NaOH activation, the adsorption capacity of methylene blue initially increases with increasing impregnation ratio, reaching an optimal point at a ratio of 4:1 for KOH and 3:1 for NaOH. Beyond these optimal values, the adsorption performance declines. This behavior can be attributed to the chemical reactions taking place during activation. Specifically, the activation of carbon with alkali hydroxides follows reactions such as:

$$6KOH + 2C \rightarrow 2K + 3H_2 + 2K_2CO_3 \quad (19)$$

$$6NaOH + 2C \rightarrow 2Na + 3H_2 + 2Na_2CO_3 \quad (20)$$

These reactions facilitate the development of micropores that are critical for adsorption. However, at high impregnation ratios, excessive gasification of carbon can lead to structural. Degradation of the adsorbent, possibly due to the widening of micropores or the collapse of the porous framework, thereby reducing the surface area and available adsorption sites.

Figure 3b investigates the influence of activation time on adsorption capacity. Here, the experimental and ANN results show a consistent trend: increasing the activation time initially enhances adsorption capacity, reaching a peak at approximately 1.5 hours for KOH-activated carbon and 2 hours for NaOH-activated carbon. This enhancement can be linked to the continued formation of activating compounds like K2CO3 and Na2CO3, which promote micropore development and increase surface area. However, extending the activation time beyond these points leads to a slight decline in adsorption capacity. This could be due to overactivation, where prolonged heating causes structural damage to the pore walls, reducing both micropore volume and surface area. This phenomenon is often associated with the collapse of smaller pores and densification of the carbon structure, resulting in reduced efficiency for methylene blue uptake.

Figure 3c presents the effect of activation temperature on the adsorption capacity. Temperature plays a crucial role in facilitating chemical activation reactions and controlling the structural evolution of the carbon matrix. The figure reveals that adsorption capacity improves with increasing activation temperature, up to an optimum of around 800°C for KOH and 700°C for NaOH. This enhancement is attributed to pore enlargement and improved surface characteristics resulting from the gasification reactions at elevated temperatures. However, when the activation temperature exceeds these limits, a sharp decrease in adsorption capacity is observed. This deterioration can be explained by the excessive gasification that occurs at high temperatures, which damages the pore structure and may lead to the coalescence or destruction of pore walls. Such degradation results in a net loss of usable surface area, thereby diminishing the adsorptive performance of the final product.

Overall, Figure 3 clearly demonstrates the critical role of synthesis parameters in tuning the adsorption capacity of activated carbon and showcases the ANN model's capability in reliably predicting adsorption performance. The agreement between the experimental and predicted results confirms that the model successfully captures the non-linear and interdependent nature of these variables, making it a valuable tool for optimization and scale-up of adsorption-based treatment processes.

A sensitivity analysis was conducted using the normalized experimental sensitivity to quantify the relative influence of impregnation ratio, activation time, and activation temperature on the adsorption capacity of KOH- and NaOH-activated carbons. The resulting sensitivity values are summarized in the bar charts presented in Fig. 4 and quantitatively describe the response of adsorption capacity to variations in each synthesis parameter.

For the KOH-activated carbon, the normalized sensitivities were 16.32 for impregnation ratio, 17.83 for activation time, and 65.85 for activation temperature. These values clearly indicate that activation temperature is the dominant parameter, exhibiting a substantially higher sensitivity than both ratio and time. While impregnation ratio and activation time contribute comparably to adsorption performance, their influence is significantly weaker than that of temperature within the investigated experimental range.

In the case of NaOH-activated carbon, the sensitivity values were 10.62 for impregnation ratio, 7.92 for activation time, and 81.45 for activation temperature. Similar to the KOH system, activation temperature shows the highest sensitivity; however,

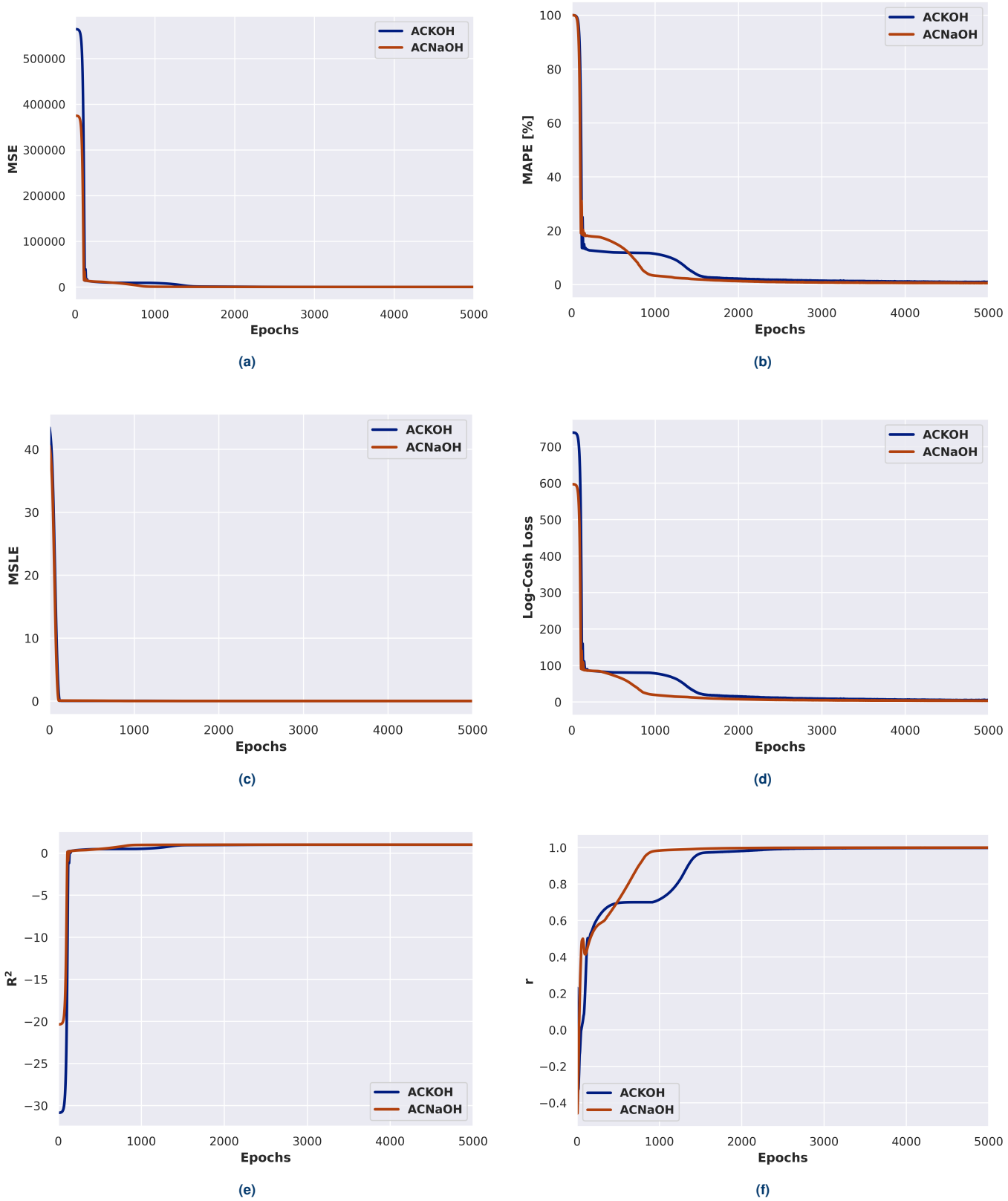

Fig. 2. A convergence of the ANN training data sets for different performance evaluation metrics (a)MSE, (b)MAPE, (c)MSLE, (d)log-cosh loss, (e)R^2 and (f)r.

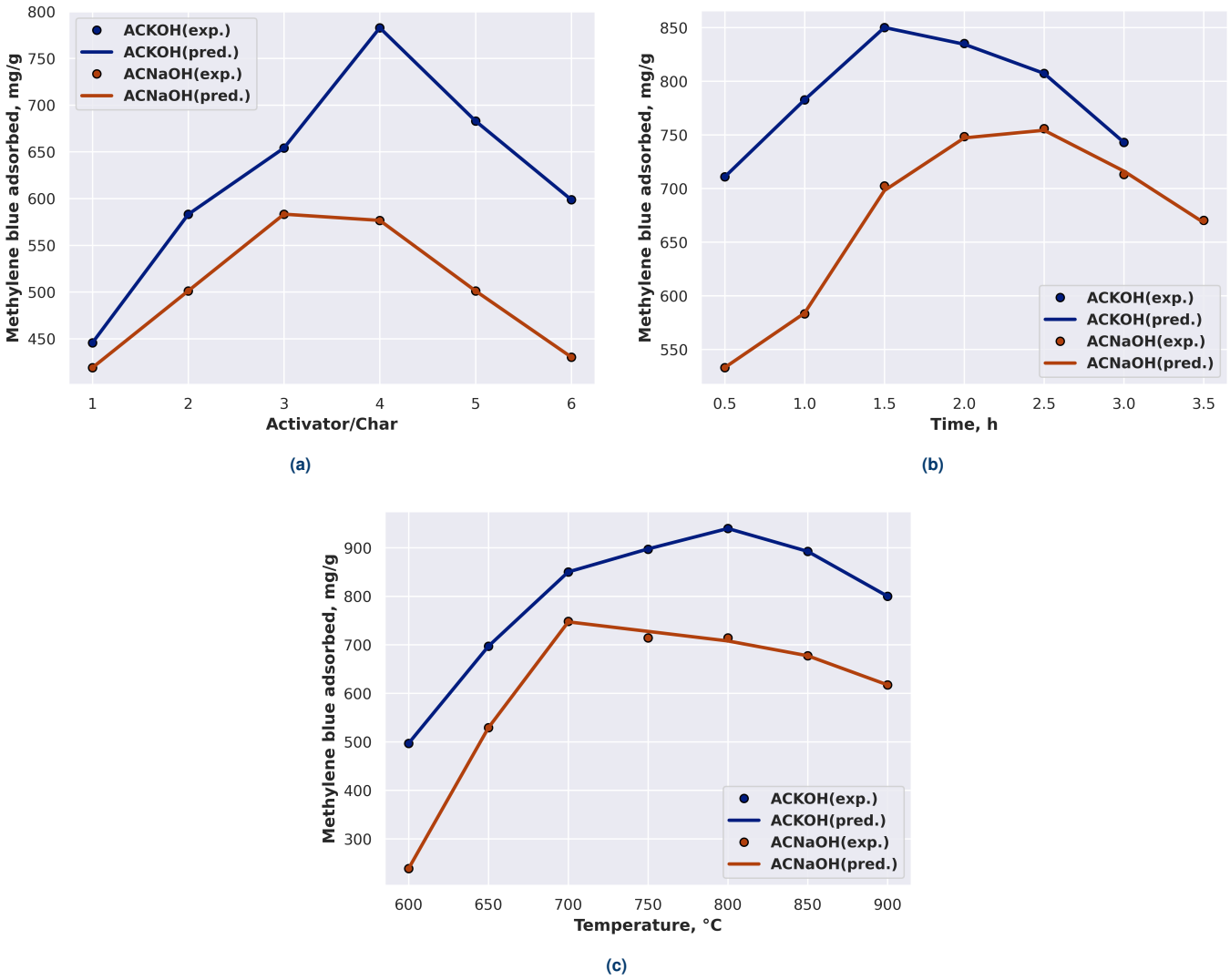

Fig. 3. Influence of pressure and temperature on concentration, illustrated through line plots (a, b), and surface plots (c) comparing experimental data and ANN predictions.

its dominance is even more pronounced for NaOH activation. The lower sensitivities associated with ratio and time suggest that adsorption capacity in NaOH-activated carbons is primarily governed by thermal effects, with comparatively limited influence from the other synthesis parameters.

A comparison between the two activating agents reveals that temperature plays a critical role in both systems, but its relative importance is higher for NaOH activation. Conversely, KOH activation exhibits more balanced sensitivities between impregnation ratio and activation time, reflecting the stronger chemical reactivity and activation efficiency of KOH during carbon synthesis.

Overall, the sensitivity analysis confirms that adsorption capacity is controlled by strongly nonlinear and coupled synthesis effects, with activation temperature being the most influential parameter for both alkali agents. These findings provide physical justification for the superior performance of the ANN model, which is capable of capturing parameter-dependent sensitivities that vary across the experimental domain, unlike quadratic regression with fixed coefficients.

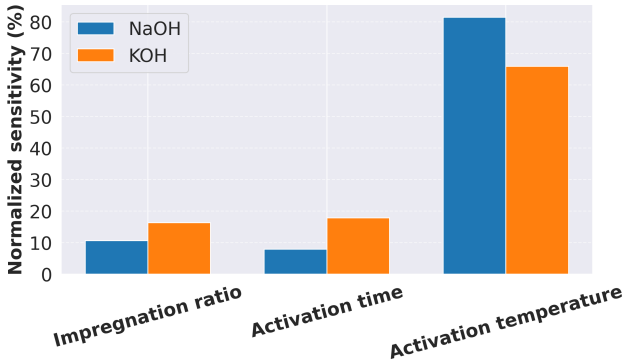

Fig. 4. Sensitivity of methylene blue adsorption to key synthesis parameters (impregnation ratio, activation time, activation temperature) for KOH- and NaOH-activated carbons.

3.3. Performance Evaluation of ANN Model

Explicit regression equations were developed for KOH- and NaOH-activated carbons to provide an interpretable baseline representation of the relationship between synthesis parameters and adsorption capacity. In both cases, a multivariate quadratic regression model was adopted, in which the adsorption capacity q (mg g-1) was expressed as a second-order polynomial function of impregnation ratio (R), activation time (t), and activation temperature (T). For KOH-activated carbon, the regression model is expressed as:

$$\begin{aligned} q_{\mathrm{KOH}} = {} & a_0^{\mathrm{KOH}} + a_1^{\mathrm{KOH}} R + a_2^{\mathrm{KOH}} t + a_3^{\mathrm{KOH}} T \\ & + a_4^{\mathrm{KOH}} R^2 + a_5^{\mathrm{KOH}} t^2 + a_6^{\mathrm{KOH}} T^2 \\ & + a_7^{\mathrm{KOH}} Rt + a_8^{\mathrm{KOH}} RT + a_9^{\mathrm{KOH}} tT \end{aligned} \tag{21}$$

Similarly, for NaOH-activated carbon, the regression equation is given by:

[h!]

Table 1. Quadratic regression coefficients for predicting adsorption capacity of KOH- and NaOH-activated carbons.

Coefficient	Term	KOH	NaOH
a_0	Intercept	−5330.364	−8283.976
a_1	(R)	−0.0868	−0.0976
a_2	(t)	−0.0322	−0.0649
a_3	(T)	15.3077	22.8672
a_4	(R^2)	−39.9275	−28.9766
a_5	(t^2)	−79.9095	−43.7408
a_6	(T^2)	−0.01117	−0.01566
a_7	(Rt)	−0.2155	−0.2921
a_8	(RT)	0.4529	0.29
a_9	(tT)	0.4425	0.3369

$$\begin{aligned} q_{\mathrm{NaOH}} = {} & a_0^{\mathrm{NaOH}} + a_1^{\mathrm{NaOH}} R + a_2^{\mathrm{NaOH}} t + a_3^{\mathrm{NaOH}} T \\ & + a_4^{\mathrm{NaOH}} R^2 + a_5^{\mathrm{NaOH}} t^2 + a_6^{\mathrm{NaOH}} T^2 \\ & + a_7^{\mathrm{NaOH}} Rt + a_8^{\mathrm{NaOH}} RT + a_9^{\mathrm{NaOH}} tT \end{aligned} \tag{22}$$

The regression coefficients were determined independently for each activating agent using least-squares fitting of the corresponding experimental datasets as shown in table 1. These quadratic models serve as physically interpretable reference models against which the predictive capability of the artificial neural network (ANN) is quantitatively and visually assessed in the subsequent scatter-plot and error-bar analyses.

Figures 5a and 5b present parity scatter plots for KOH and NaOH activated carbons, respectively, comparing the experimentally measured adsorption capacity with predictions obtained from the quadratic regression and artificial neural network (ANN) models. The experimental adsorption capacity is shown on the horizontal axis, while the predicted values are plotted on the vertical axis, with the 45° diagonal line indicating ideal agreement.

For both activating agents, the quadratic regression model exhibits increased dispersion around the parity line, particularly at higher adsorption capacities and at extreme combinations of synthesis parameters. Although the regression model captures the overall trend of the data, these deviations indicate its limited ability to represent the complex and nonlinear interactions among impregnation ratio, activation time, and activation temperature.

In contrast, the ANN predictions are more closely aligned with the parity line across the full range of adsorption capacities for both KOH and NaOH. The tighter clustering of points demonstrates the ANN's improved capability to model nonlinear behavior and maintain predictive accuracy under varying synthesis conditions. This comparison indicates that, while quadratic regression provides a reasonable approximation, the ANN model offers superior predictive consistency and generalization performance.

In Figures 6a and 6b, error bars are included to quantify the local prediction uncertainty associated with each model for KOH and NaOH, respectively. For the quadratic regression model, the error bars show larger magnitudes and greater vari-

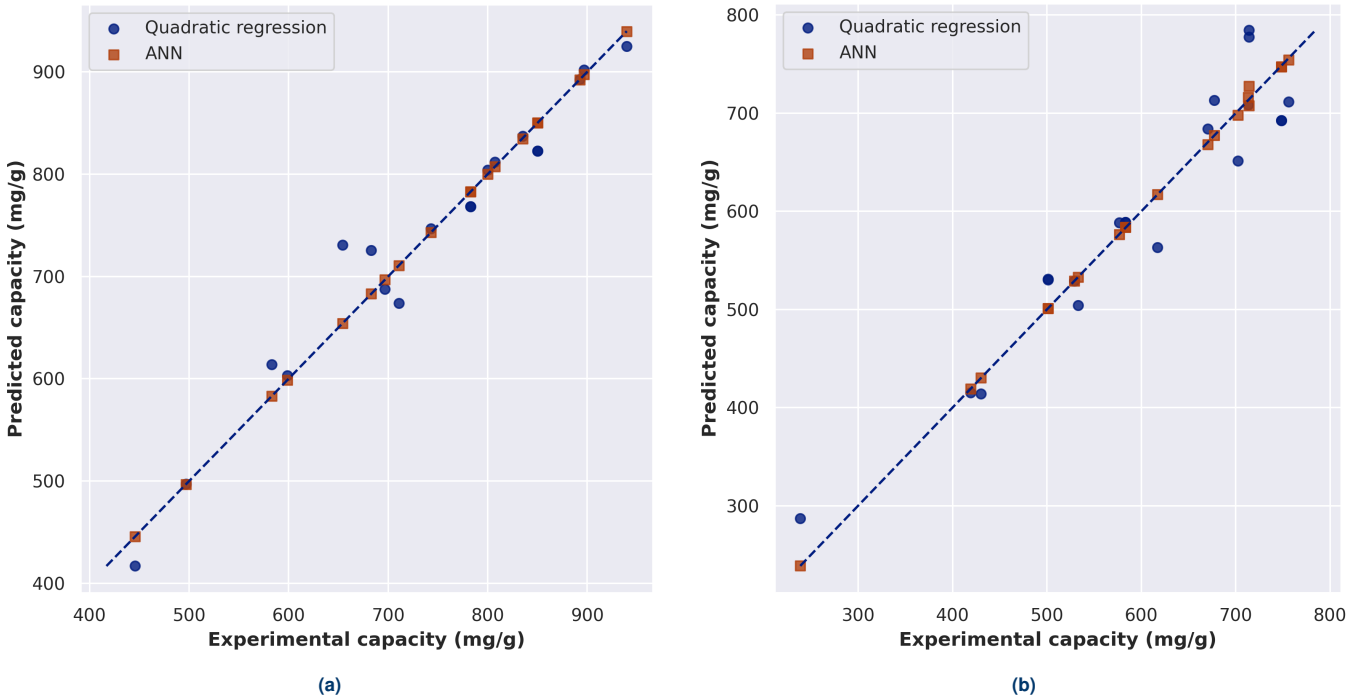

Fig. 5. Parity plots of experimental and predicted adsorption capacity for (a) KOH-activated and (b) NaOH-activated carbons using quadratic regression and ANN models.

ability across the investigated parameter space, indicating that prediction uncertainty depends strongly on the operating conditions. This non-uniform behavior reflects the sensitivity of the regression model to parameter changes and its limited flexibility in describing nonlinear response surfaces.

By comparison, the ANN model exhibits smaller and more uniformly distributed error bars, indicating reduced prediction uncertainty and more stable performance across different synthesis conditions. The consistent error magnitude suggests that the ANN maintains comparable prediction accuracy throughout the parameter space, rather than being reliable only near specific experimental conditions. The reduced uncertainty associated with the ANN predictions further supports its robustness and suitability for predictive modeling and process optimization of alkali-activated carbons.

Figure 7 illustrates a comprehensive comparison of the artificial neural network (ANN) model's performance across different impregnation ratio values (ranging from 1 to 6) for two chemical activation agents: potassium hydroxide (KOH) and sodium hydroxide (NaOH). The performance was evaluated using six distinct metrics, namely MSE), MAPE, MSLE, Log-Cosh Loss, R^2, and r. Each subfigure (7a - 7f) presents bar charts that depict how these performance metrics vary in response to changing impregnation ratios.

In Fig. 7a, which represents MSE, the ANN model trained on KOH-activated carbon data exhibits the lowest MSE value (3.2×10^{-2}) at an impregnation ratio of 3, indicating minimal prediction error at this point. The highest MSE for KOH is observed at a ratio of 4 (7.5×10^{-2}), suggesting increased variance between predicted and actual values. For NaOH activation, the lowest MSE (4.1×10^{-2}) occurs at a ratio of 5, while the highest (7.2×10^{-2}) appears at a ratio of 1. These variations imply that the optimal impregnation ratio for minimizing prediction error differs depending on the chemical activator used.

Figure 7b presents MAPE trends, revealing that the KOH model performs best (lowest MAPE of 4.2×10^{-1}) at an impregnation ratio of 2, with performance deteriorating at higher ratios (e.g.,8.5×10^{-1} at ratio 5). In contrast, the NaOH model achieves its best performance at a ratio of 4 with a MAPE of 3.1×10^{-1}, indicating more accurate predictions in this condition. Fluctuations in MAPE values across different ratios highlight the sensitivity of the ANN's relative prediction accuracy to the synthesis parameter.

In Fig. 7c, which depicts MSLE, the KOH-based model again performs best at an impregnation ratio of 5 with a value of 4.2×10^{-6}, while its worst performance (8.2×10^{-6}) is recorded at a ratio of 3. For NaOH, the most favorable MSLE is 4.1×10^{-6} at a ratio of 1, whereas the highest error (9.2×10^{-6}) is noted at a ratio of 3. These results further support that the learning model's ability to capture relative errors in log scale is highly dependent on the specific activation method and ratio applied.

Fig. 7d examines the log-cosh loss metric, which behaves similarly to MSE but is more robust to outliers. For KOH, the lowest log-cosh loss (4.2×10^{-2}) is achieved at a ratio of 3, while the highest (8.5×10^{-2}) is at a ratio of 5. In contrast, the NaOH model attains its best performance (5.2×10^{-2}) at a ratio of 4 and shows the poorest outcome (9.1×10^{-2}) at a ratio of 3. The consistency between MSLE and log-cosh trends,

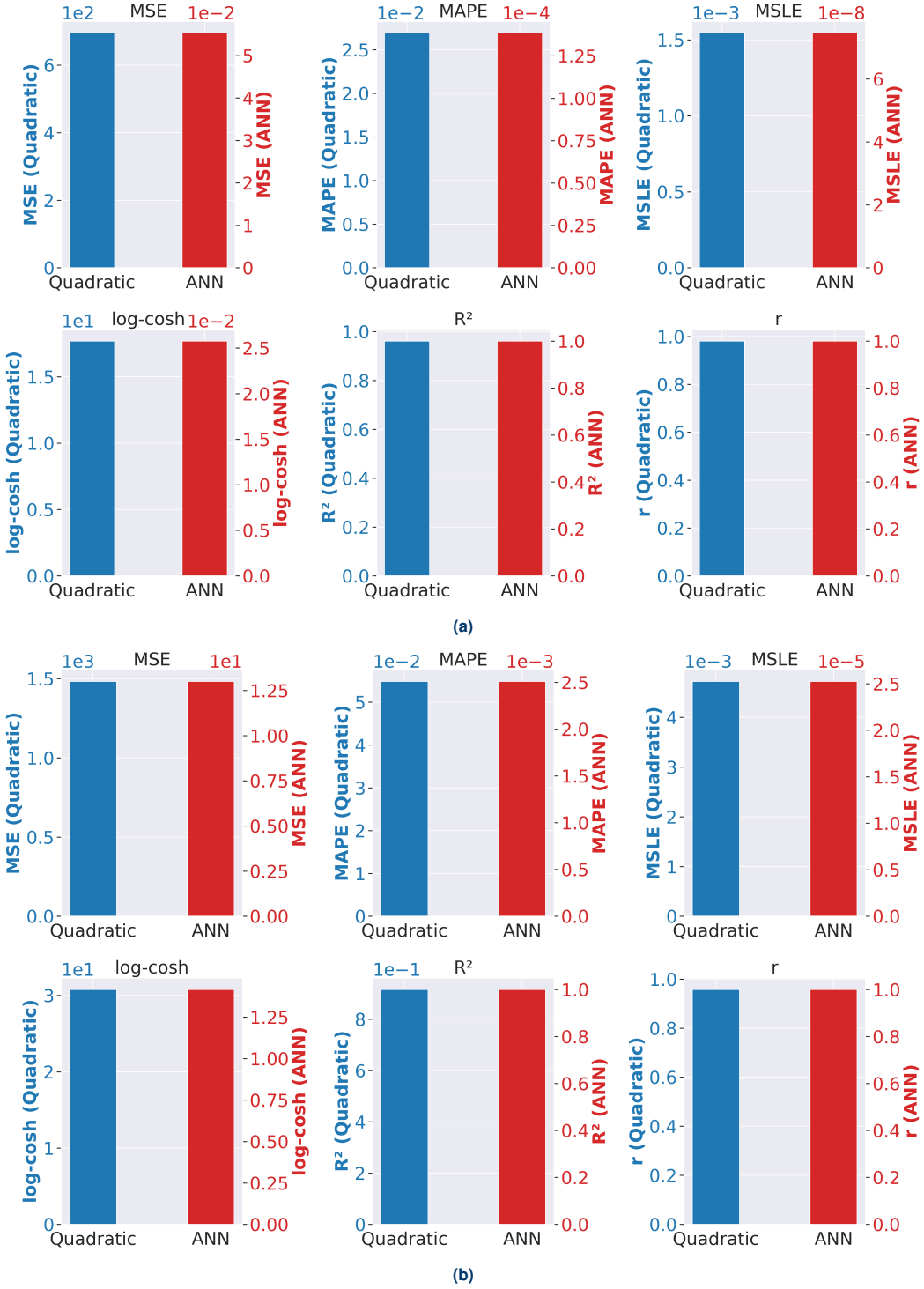

Fig. 6. Error-metric comparison between quadratic regression and ANN models for (a) KOH-activated and (b) NaOH-activated carbons.

especially at a ratio of 3 for NaOH, highlights a potential challenge in prediction accuracy around this synthesis condition.

Turning to R^2, as shown in Fig. 7e, the KOH model demonstrates outstanding regression performance, particularly at an impregnation ratio of 5, achieving an R^2 of 0.99, indicating near-perfect correlation between predicted and actual values. The lowest R^2 for KOH (0.94) occurs at a ratio of 3. For NaOH, the best R^2 (0.975) is seen at a ratio of 6, suggesting that higher impregnation levels may benefit prediction fidelity in this case, while the lowest value (0.94) is at a ratio of 4.

Finally, Fig. 7f presents the Pearson correlation coefficient (r), which measures the linear relationship between predicted and actual adsorption capacities. For KOH, the highest correlation (0.98) occurs at a ratio of 3, closely followed by values above 0.96 at most other ratios. The NaOH model records its peak correlation (0.98) at a ratio of 6, which aligns well with the corresponding R^2 value. These findings collectively suggest strong agreement between predicted and actual trends, with KOH showing more consistency across various ratios.

In summary, Fig. 7 provides critical insights into how the impregnation ratio impacts ANN model performance for both KOH and NaOH-activated carbon systems. The observed variations across metrics reinforce the importance of optimizing synthesis parameters not only for experimental adsorption capacity but also for achieving high predictive accuracy in data-driven models. The results demonstrate that while KOH generally exhibits more consistent and higher performance, NaOH also yields competitive results at certain impregnation levels, particularly at higher ratios.

4. CONCLUSIONS

This study demonstrated the successful application of a deep multilayer perceptron (MLP) artificial neural network to predict the adsorption capacity of methylene blue onto alkali-activated carbons synthesized using potassium hydroxide (KOH) and sodium hydroxide (NaOH). By combining experimental adsorption data with a data-driven modeling approach, the developed ANN accurately captured the complex and nonlinear relationships between key synthesis parameters—impregnation ratio, activation temperature, and activation time—and adsorption performance. The optimized deep network, trained using backpropagation with the ADAM optimizer, exhibited excellent convergence behavior and strong generalization capability for both activation routes. The close agreement between experimental and predicted results confirms the robustness of the proposed framework and its suitability as an efficient predictive tool for activated carbon design and optimization.

Based on the obtained results, the main conclusions of this study can be summarized as follows:

- A deep MLP-ANN model with ten hidden layers and fourteen neurons per layer was successfully developed to predict methylene blue adsorption capacity with high accuracy.
- Separate ANN models for KOH- and NaOH-activated carbons demonstrated strong predictive performance, with slightly superior accuracy observed for KOH-activated samples.
- The ANN effectively modeled highly nonlinear interactions between synthesis parameters without requiring explicit mechanistic assumptions.
- Impregnation ratio, activation temperature, and activation time were identified as critical parameters governing pore development and adsorption efficiency.
- Optimal synthesis conditions were successfully captured by the ANN, including the negative impact of overactivation at excessive temperatures or impregnation ratios.
- The proposed ANN framework significantly reduces experimental effort and can be used as a rapid screening and optimization tool for adsorption materials.
- This approach provides a solid foundation for extending machine-learning-based modeling to other adsorbents, adsorbates, and activation strategies in environmental applications.

DATA AVAILABILITY

All data generated or analyzed during this study are included in this published article.

REFERENCES

[1] I. Khan, K. Saeed, I. Zekker, B. Zhang, A. H. Hendi, A. Ahmad, S. Ahmad, N. Zada, H. Ahmad, L. A. Shah *et al.*, "Review on methylene blue: its properties, uses, toxicity and photodegradation," *Water*, vol. 14, no. 2, p. 242, 2022.

[2] P. O. Oladoye, T. O. Ajiboye, E. O. Omotola, and O. J. Oyewola, "Methylene blue dye: Toxicity and potential elimination technology from wastewater," *Results in Engineering*, vol. 16, p. 100678, 2022.

[3] M. F. Valiyathur, M. S. Sakvai, S. Mithra, S. A. Majeed, A. B. Kottur, A. S. S. Hameed, and A. A. Raza, "Photocatalytic and toxicity assessment of alginate reinforced zno-g-c3n4 photocatalyst for the degradation of methylene blue–a sustainable strategy," *International Journal of Biological Macromolecules*, vol. 298, p. 139935, 2025.

[4] K. Arya, A. Kumar, A. Sharma, K. Thakur, R. Kumar, S. K. Mehta, S. Singh, V. Kumar, and R. Kataria, "Light-assisted synergistic effect of zn-mof@ rgo nanocomposite for methylene blue degradation and toxicity analysis to water reclamation," *Inorganic Chemistry Communications*, vol. 173, p. 113768, 2025.

[5] V. M. Furqaan, S. Mithra, S. A. Majeed, K. A. Basha, A. S. S. Hameed, and S. M. Safiullah, "Alginate/cuo-gc3n4 composite: a novel, reusable, non-toxic photocatalyst for methylene blue degradation," *Environmental Science and Pollution Research*, vol. 32, no. 28, pp. 16 912–16 930, 2025.

[6] N. Nipu, L. Wei, J. Thomas, and J. A. Mennigen, "Methylene blue is a widely used antifungal agent that confounds behavioral toxicity assays in larval zebrafish," *Environmental Science & Technology Letters*, vol. 12, no. 2, pp. 130–136, 2025.

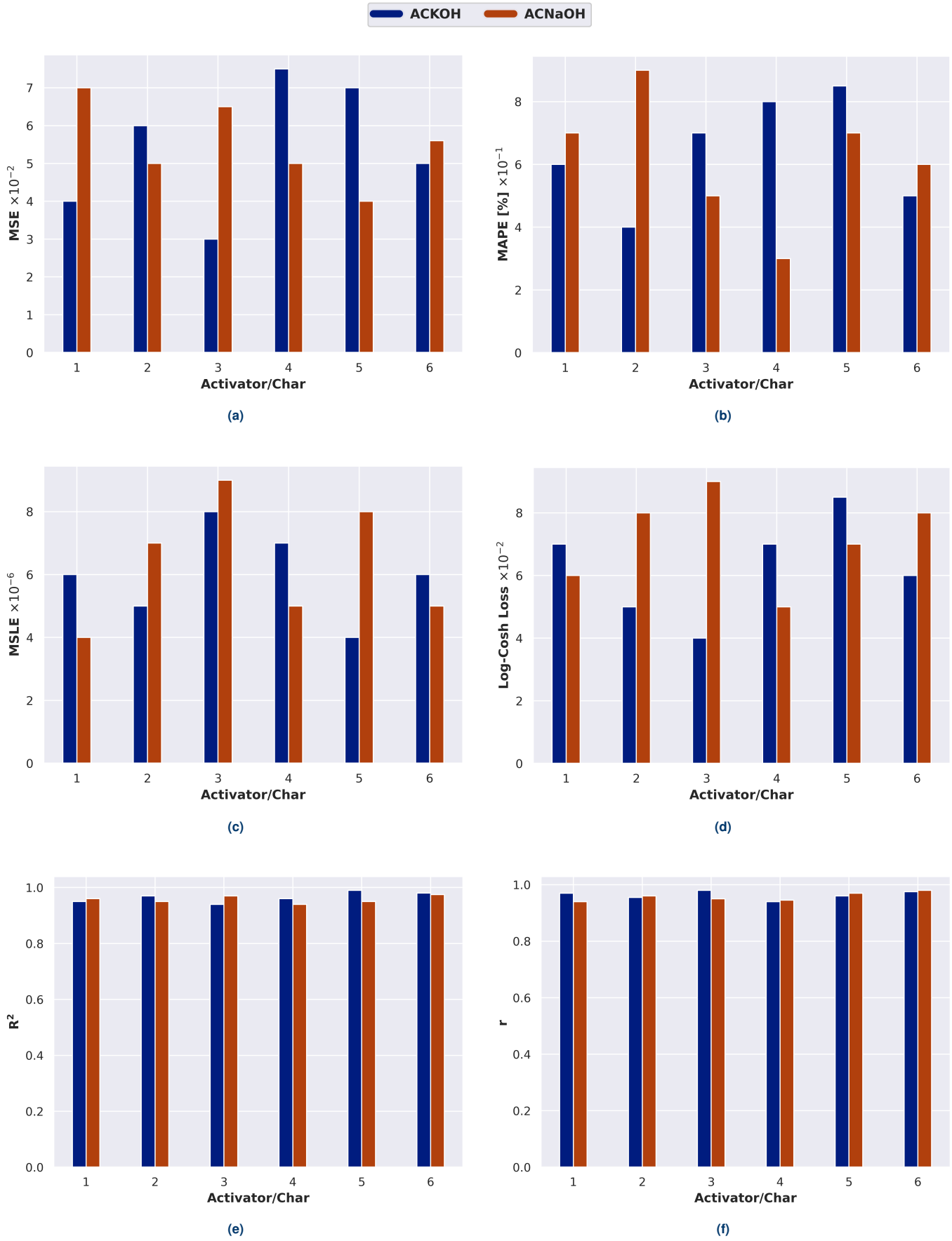

Fig. 7. Regression statistics of the present ANN model using different performance evaluation metrics (a)MSE, (b)MAPE, (c)MSLE, (d)log-cosh loss, (e)R^2 and (f)r.

[7] D. Bhatia, N. R. Sharma, J. Singh, and R. S. Kanwar, "Biological methods for textile dye removal from wastewater: A review," *Critical Reviews in Environmental Science and Technology*, vol. 47, no. 19, pp. 1836–1876, 2017.

[8] T. Shindhal, P. Rakholiya, S. Varjani, A. Pandey, H. H. Ngo, W. Guo, H. Y. Ng, and M. J. Taherzadeh, "A critical review on advances in the practices and perspectives for the treatment of dye industry wastewater," *Bioengineered*, vol. 12, no. 1, pp. 70–87, 2021.

[9] B. M. Adesanmi, Y.-T. Hung, H. Paul, and C. Huhnke, "Comparison of dye wastewater treatment methods: A review." *GSC Advanced Research and Reviews, 10 (2)*, vol. 10, no. 2, p. 126, 2022.

[10] G. Bal and A. Thakur, "Distinct approaches of removal of dyes from wastewater: A review," *Materials Today: Proceedings*, vol. 50, pp. 1575–1579, 2022.

[11] H. Kumari, Sonia, Suman, R. Ranga, S. Chahal, S. Devi, S. Sharma, S. Kumar, P. Kumar, S. Kumar *et al.*, "A review on photocatalysis used for wastewater treatment: dye degradation," *Water, Air, & Soil Pollution*, vol. 234, no. 6, p. 349, 2023.

[12] Q. Ghzal, T. Javed, A. N. Zghair, M. N. Haider, M. J. Abed, L. S. Jasim, and R. Iftikhar, "Sustainable dye wastewater treatment: A review of effective strategies and future directions," *Physical Chemistry Research*, vol. 13, no. 3, pp. 479–509, 2025.

[13] A. Bhatnagar, W. Hogland, M. Marques, and M. Sillanpää, "An overview of the modification methods of activated carbon for its water treatment applications," *Chemical Engineering Journal*, vol. 219, pp. 499–511, 2013.

[14] M. S. Muzarpar, A. Leman, N. Maghpor, N. N. M. Hassan, and N. Misdana, "The adsorption mechanism of activated carbon and its application-a review," *International Journal of Advanced Technology in Mechanical, Mechatronics and Materials*, vol. 1, no. 3, pp. 118–124, 2020.

[15] E. I. Ugwu and J. C. Agunwamba, "A review on the applicability of activated carbon derived from plant biomass in adsorption of chromium, copper, and zinc from industrial wastewater," *Environmental monitoring and assessment*, vol. 192, no. 4, p. 240, 2020.

[16] R. Rashid, I. Shafiq, P. Akhter, M. J. Iqbal, and M. Hussain, "A state-of-the-art review on wastewater treatment techniques: the effectiveness of adsorption method," *Environmental Science and Pollution Research*, vol. 28, no. 8, pp. 9050–9066, 2021.

[17] S. T. Al-Asadi, Z. H. Mussa, F. F. Al-Qaim, H. Kamyab, H. F. S. Al-Saedi, I. F. Deyab, and N. J. Kadhim, "A comprehensive review of methylene blue dye adsorption on activated carbon from edible fruit seeds: A case study on kinetics and adsorption models," *Carbon Trends*, p. 100507, 2025.

[18] S. R. Dumbre, V. K. Kadam, E. M. Kabadi, R. N. Shirsat, and S. S. Pingale, "A review on recent advances in biowaste-based activated carbon nanomaterials for wastewater treatment," *Current Green Chemistry*, 2025.

[19] Grand View Research, "Activated carbon market size, share & trends analysis report, 2026–2033," https://www.grandviewresearch.com/industry-analysis/activated-carbon-market, 2025, accessed: March 15, 2025.

[20] S. Guo, Z. Zou, Y. Chen, X. Long, M. Liu, X. Li, J. Tan, and R. Chen, "Synergistic effect of hydrogen bonding and π-π interaction for enhanced adsorption of rhodamine b from water using corn straw biochar," *Environmental Pollution*, vol. 320, p. 121060, 2023.

[21] X. Chen, M. Li, J. He, Y. Wu, J. Sun, and X. Wen, "Waste cotton-based activated carbon with excellent adsorption performance towards dyes and antibiotics," *Chemosphere*, vol. 376, p. 144292, 2025.

[22] F. Ebrahimzadeh and A. Akbari, "Investigation the adsorption mechanisms, chemical resistance and mechanical strength of the synthesized chitosan/activated carbon composite in methylene blue removal," *Scientific Reports*, vol. 15, no. 1, p. 37820, 2025.

[23] W. Ji, H. Jin, H. Wang, S. Tabassum, Y. Lou, X. Fan, M. Ren, and J. Wang, "Elucidating the dominant role of π–π interactions in methylene blue removal via porous biochar: A synergistic approach of experimental and theoretical mechanistic insights," *Colloids and Surfaces A: Physicochemical and Engineering Aspects*, vol. 715, p. 136615, 2025.

[24] S. Sawasdee and P. Watcharabundit, "Mechanistic insights into adsorption of methylene blue and methyl orange using cassava rhizome activated carbon: Adsorption, characterization and reusability," *Trends in Sciences*, vol. 22, no. 12, pp. 10 751–10 751, 2025.

[25] D.-C. Lv, M.-R. Chen, M.-R. Song, G.-C. Jiang, and Z.-M. Wang, "Beyond electrostatic interaction: Ball milling-induced dominance of pore filling and π-π stacking for methylene blue adsorption on tobacco stem derived activated carbon," *Journal of Water Process Engineering*, vol. 81, p. 109435, 2026.

[26] S. Mohamed Nasser, M. Abbas, and M. Trari, "Understanding the rate-limiting step adsorption kinetics onto biomaterials for mechanism adsorption control," *Progress in Reaction Kinetics and Mechanism*, vol. 49, p. 14686783241226858, 2024.

[27] Z. Heidarinejad, M. H. Dehghani, M. Heidari, G. Javedan, I. Ali, and M. Sillanpää, "Methods for preparation and activation of activated carbon: a review," *Environmental Chemistry Letters*, vol. 18, no. 2, pp. 393–415, 2020.

[28] M. Sevilla, N. Díez, and A. B. Fuertes, "More sustainable chemical activation strategies for the production of porous carbons," *ChemSusChem*, vol. 14, no. 1, pp. 94–117, 2021.

[29] N. E. Williams, O. A. Oba, and N. P. Aydinlik, "Modification, production, and methods of koh-activated carbon," *ChemBioEng Reviews*, vol. 9, no. 2, pp. 164–189, 2022.

[30] T. W. Chew, P. S. H'Ng, B. C. T. G. Luqman Chuah Abdullah, K. L. Chin, C. L. Lee, B. M. S. Mohd Nor Hafizuddin, and L. TaungMai, "A review of bio-based activated carbon properties produced from differ-

ent activating chemicals during chemicals activation process on biomass and its potential for malaysia," *Materials*, vol. 16, no. 23, p. 7365, 2023.

[31] N. Panwar and A. Pawar, "Influence of activation conditions on the physicochemical properties of activated biochar: A review," *Biomass Conversion and Biorefinery*, vol. 12, no. 3, pp. 925–947, 2022.

[32] R. Murugavel, A. A. Rownaghi, and F. Rezaei, "Effect of alkali metal functionalization on hydrogen storage performance of highly porous activated carbons," *Energy & fuels*, vol. 37, no. 23, pp. 19 292–19 303, 2023.

[33] N. P. Ponomarev, "A salt and alkali synergy for synthesising active carbons from lignin: porosity development and techno-economic assessment," 2023.

[34] X. Tian, Z. Chen, J. Hou, and Z. Li, "Electrochemical properties of porous carbon derived from coal gasification fine ash via low-temperature alkaline fusion and koh activation," *Journal of Energy Storage*, vol. 75, p. 109557, 2024.

[35] V. Pusarapu, C. Stoll, L. Huntington, P. Patel, A. Mamidala, and G. Gadikota, "4 potassium and nickel-catalyzed alkaline thermal graphitization for sustainable co-production of porous graphitic carbon for lithium batteries and syngas," *Mechanistic Insights Underlying the Valorization of Biogenic Resources to Co-produce Sustainable Fuels and Carbonaceous Products*, p. 45, 2025.

[36] N.-B. Mihaly, M. Simon-Varhelyi, and V. M. Cristea, "Data-driven modelling based on artificial neural networks for predicting energy and effluent quality indices and wastewater treatment plant optimization," *Optimization and Engineering*, vol. 23, no. 4, pp. 2235–2259, 2022.

[37] M. Parsaei, E. Roudbari, F. Piri, A. El-Shafay, C.-H. Su, H. C. Nguyen, M. Alashwal, S. Ghazali, and M. Algarni, "Neural-based modeling adsorption capacity of metal organic framework materials with application in wastewater treatment," *Scientific Reports*, vol. 12, no. 1, p. 4125, 2022.

[38] M. Zafar, A. Aggarwal, E. R. Rene, K. Barbusiński, B. Mahanty, and S. K. Behera, "Data-driven machine learning intelligent tools for predicting chromium removal in an adsorption system," *Processes*, vol. 10, no. 3, p. 447, 2022.

[39] S. Zhang, Y. Jin, W. Chen, J. Wang, Y. Wang, and H. Ren, "Artificial intelligence in wastewater treatment: A data-driven analysis of status and trends," *Chemosphere*, vol. 336, p. 139163, 2023.

[40] W. Dai, J.-W. Pang, J. Ding, J.-h. Wang, C. Xu, L.-Y. Zhang, N.-Q. Ren, and S.-S. Yang, "Integrated real-time intelligent control for wastewater treatment plants: data-driven modeling for enhanced prediction and regulatory strategies," *Water Research*, vol. 274, p. 123099, 2025.

[41] Y.-P. Song, W.-Z. Wang, Y.-Q. Wang, W.-X. Yin, J.-J. Chen, H.-R. Xu, H.-Y. Cheng, F. Ma, H.-T. Wang, A.-J. Wang *et al.*, "Data-driven differentiable model for dynamic prediction and control in wastewater treatment," *Water Research*, p. 123772, 2025.

[42] K. N. Pai, T. T. Nguyen, V. Prasad, and A. Rajendran, "Experimental validation of an adsorbent-agnostic artificial neural network (ann) framework for the design and optimization of cyclic adsorption processes," *Separation and Purification Technology*, vol. 290, p. 120783, 2022.

[43] H. E. Reynel-Ávila, I. A. Aguayo-Villarreal, L. L. Diaz-Muñoz, J. Moreno-Pérez, F. J. Sánchez-Ruiz, C. K. Rojas-Mayorga, D. I. Mendoza-Castillo, and A. Bonilla-Petriciolet, "A review of the modeling of adsorption of organic and inorganic pollutants from water using artificial neural networks," *Adsorption Science & Technology*, vol. 2022, p. 9384871, 2022.

[44] S. M. Alardhi, S. S. Fiyadh, A. D. Salman, and M. Adelikhah, "Prediction of methyl orange dye (mo) adsorption using activated carbon with an artificial neural network optimization modeling," *Heliyon*, vol. 9, no. 1, 2023.

[45] J. Pellegrini and J. de Celis, "Refinement of a kinetic adsorption model through artificial intelligence," *Brazilian Journal of Development*, vol. 10, no. 12, pp. e75 662–e75 662, 2024.

[46] R. Tariq, M. Abatal, J. Vargas, and A. Y. Vázquez-Sánchez, "Deep learning artificial neural network framework to optimize the adsorption capacity of 3-nitrophenol using carbonaceous material obtained from biomass waste," *Scientific Reports*, vol. 14, no. 1, p. 20250, 2024.

[47] M. F. da Costa, R. d. S. Araújo, A. R. Silva, L. Pereira, and G. M. Silva, "Predictive artificial neural networks as applied tools in the remediation of dyes by adsorption—a review," *Applied Sciences*, vol. 15, no. 5, p. 2310, 2025.

[48] F. Fathalian, S. Aarabi, A. Ghaemi, and A. Hemmati, "Intelligent prediction models based on machine learning for co2 capture performance by graphene oxide-based adsorbents," *Scientific Reports*, vol. 12, no. 1, p. 21507, 2022.

[49] W. Guo, J. Liu, F. Dong, R. Chen, J. Das, W. Ge, X. Xu, and H. Hong, "Deep learning models for predicting gas adsorption capacity of nanomaterials," *Nanomaterials*, vol. 12, no. 19, p. 3376, 2022.

[50] P. Mehrmohammadi and A. Ghaemi, "Investigating the effect of textural properties on co2 adsorption in porous carbons via deep neural networks using various training algorithms," *Scientific Reports*, vol. 13, no. 1, p. 21264, 2023.

[51] M. Shayanmehr, S. Aarabi, A. Ghaemi, and A. Hemmati, "A data driven machine learning approach for predicting and optimizing sulfur compound adsorption on metal organic frameworks," *Scientific Reports*, vol. 15, no. 1, p. 3138, 2025.

[52] A. Gadalla, S. Younis, M. Fahmy, N. Ibiari, and J. Y. Farah, "Preparation of porous activated carbons from rice husk with alkali activation," *Eurasian Chemico-Technological Journal*, vol. 9, no. 2, pp. 139–145, 2007.